ELSEVIER

Journal of Nuclear Materials 277 (2000) 67–81

journal of nuclear materials

www.elsevier.nl/locate/jnucmat

On the theory of fission gas bubble evolution in irradiated UO_2 fuel

M.S. Veshchunov*

Nuclear Safety Institute (IBRAE), Russian Academy of Sciences, B-Tul'skaya 52, Moscow 113191, Russian Federation

Received 13 April 1999; accepted 7 June 1999

Abstract

The standard approaches for modelling of the intra- and intergranular bubbles evolution in the UO_2 fuel are critically analysed on the basis of available experimental data. It is demonstrated that the main disadvantage of the simplified treatment of the problem by the standard models can be associated with underestimation of the radiation effects at low temperatures (below 1500°C) and thermal effects at high temperatures (above 1500°C). The presented analysis allows a quantitative description of the bubble nucleation mechanism, adequate modelling of the bubble diffusion growth, and evaluation of the intragranular bubble number density and stable size attained under steady irradiation conditions.

1. Introduction

The influence of fission gases generated in oxide fuels during irradiation on fuel performance has been the subject of many investigations over the past 40 yr. The fission inert gases are known to precipitate into bubbles. The growing bubbles cause the fuel to swell. In addition, fission gas bubbles retained in the fuel on grain surfaces and edges can cause radical changes in the fuel microstructure. These changes in the fuel microstructure can then result in an enhanced gas release and fuel swelling.

Any model that attempts a realistic description of fission gas release and swelling as a function of fuel-fabrication variables and a wide range of reactor operating conditions must treat fission gas release and fuel swelling as coupled phenomena and must include many mechanisms influencing fission gas behaviour. Currently, the most advanced models which include the mechanistic description of these phenomena are the numerical codes GRASS-SST [1], FASTGRASS [2], VICTORIA [3]. These codes consider the effects of production of gas from fissioning uranium, bubble nucleation, a realistic equation of state for xenon, lattice gas diffusivities based on experimental observations, bubble growth, migration and coalescence, re-solution, temperature and temperature gradients, interlinked porosity, etc.

However, some of the code models seem to be oversimplified and do not allow a realistic description of many observed phenomena. The basic assumption of these models is connected with the bubble state description by the so-called 'capillarity' relation and the quasi-stationary approximation for the bubble growth based on this relation. Such an approach radically simplifies the theory, since in this case the defect structure of the crystal (including point defects, such as vacancies and interstitials, and extended defects, such as dislocations) is practically excluded from consideration (with the exception of some simple effects such as athermal behaviour of the gas and uranium atom diffusivities in the irradiated crystal). However, this consideration is well grounded only for the description of equilibrium crystals and generally fails under irradiation conditions when the fuel matrix is oversaturated with the point defects (vacancies and interstitials).

In parallel to the fuel behaviour investigations, extensive experimental and theoretical studies of the metal crystal behaviour under irradiation conditions were carried out (e.g. [4–6]). Results of these investigations unambiguously demonstrated a great influence of point

* Corresponding author. Tel.: +7-095 955 2218; fax: +7-095 958 0040.

E-mail address: vms@ibrae.ac.ru (M.S. Veshchunov).

0022-3115/00/$ - see front matter
PII: S0022-3115(99)00136-1

defects generated under similar (to the fuel) irradiation conditions on the bubble nucleation and growth in metals. However, these results were mainly unaccounted in the models dealing with the bubble porosity evolution in the oxide fuel, despite the general character of many theoretical conclusions.

In the present paper an attempt is made to extend the general approach of the irradiated metal description to the modelling of the bubble behaviour in the UO_2 fuel. It is demonstrated that in some cases the standard approach for the bubble behaviour in the fuel (based on the capillarity relation) can be really used (for example, at high temperatures above 1500°C). However, in other cases a more realistic description of bubble interactions with non-equilibrium point defects must be applied. Hence, the radiation effects unaccounted in the models [1–3] become especially important in the case of the large bubbles evolution (observed on the grain faces and, after temperature transients, in the bulk of the grains), since in these cases the mechanism and rate of the fuel swelling and gas release through the open porosity may be strongly underestimated by the standard approach (see Sections 2 and 5).

Naturally, a similar approach to the metal description leads sometimes to quite different results for the fuel, since many parameters of the two systems differ significantly. For example, the mechanism of small bubble interactions with fission fragments in the fuel, associated with the bubble relaxation in the short living ($\approx 10^{-11}$ s) molten zone of fission tracks (considered in Section 2), can strongly change the intragranular porosity evolution. Or, a relatively small value of the self-diffusion coefficient in the fuel (in comparison with that in metals) leads to a significant extension of the initial, so-called 'recombination' stage of irradiation when the main sink of point defects is their mutual recombination. As a result, this allows the direct calculation of the bubble nucleation factor (determined in the codes [1–3] as a default value varying in a wide range), or a natural explanation of the stabilisation of the bubble number density observed under steady irradiation conditions at $T \leqslant 1500$°C and its self-consistent calculation (Section 3).

On the other hand, in the case of high temperatures ($\geqslant 1500$°C) when radiation effects in the fuel can be mainly neglected, the codes [1–3] generally underestimate thermal effects in the fuel, namely, they do not consider the thermal resolution of gas atoms from bubbles. These effects strongly influence the bubble nucleation mechanism which, at these temperatures, becomes associated with the fluctuation formation of a finite size critical nucleus as well as the bubble evolution in a late stage of irradiation when the thermal resolution apparently determines the observed stabilisation of the bubble radius and number density (Section 4).

2. Intragranular porosity

Electron microscope examinations as well as conventional optical metallography, scanning electron microscopy and replica techniques, of uranium dioxide irradiated to doses $\geqslant 10^{19}$ fissions/cm^3 at temperatures in excess of 800°C have shown high concentrations (10^{17}–10^{18} cm^{-3}) of small intragranular fission gas bubbles. The distribution of the fission gas bubbles is of interest because it influences swelling and gas release. For example, in conditions in which the gas does not precipitate or forms very small bubbles, the gaseous component of swelling will be less than in the case of large (low pressure) bubbles. The precipitation of intragranular gas bubbles will reduce the gas atom concentration in the lattice and will reduce gas release by atomic diffusion.

2.1. Standard approach

In the majority of the currently existing models for the fission gas behaviour in the UO_2 fuel, the mechanical equilibrium state with respect to surface capillary forces of bubbles is expressed by the capillarity relation:

$$p - p_h = 2\gamma/R, \tag{1}$$

where p is the internal gas pressure, p_h the external hydrostatic pressure, R the radius of the bubble, γ the surface energy, is the usual approximation for the description of the growing intragranular bubbles (e.g. see [1–3,7–9]). In the case of the deviation from this state, for example, due to coalescence of two bubbles, it is proposed that the newly formed bubble quickly attains the equilibrium state after some characteristic relaxation time by the vacancy diffusion mechanism. This approach is usually based on the kinetic equation for the diffusional growth of bubbles [10]:

$$dR/dt = (D_u/R)\{1 - \exp[(p - p_h - 2\gamma/R)\Omega/kT]\}, \tag{2}$$

where $D_u \approx D_v c_v$ is the U atom self-diffusion coefficient, D_v and c_v the vacancy diffusion coefficient and bulk concentration, respectively; Ω is the vacancy volume in the UO_2 matrix ($\Omega \approx 4.1 \times 10^{-23}$ cm^3). In accordance with Eq. (2) the quasi-stationary state of a bubble ($dR/dt = 0$) is characterised by the capillarity relation, Eq. (1).

2.2. Correct description

However, such an approach becomes incorrect in many cases, since Eq. (2) is valid only for the equilibrium crystals, i.e. when the concentration c_v of vacancies does not exceed the thermal equilibrium value c_v^{eq}. Otherwise, for crystals oversaturated with the

non-equilibrium vacancies, a more adequate expression has the form [11]

$$\mathrm{d}R/\mathrm{d}t = (D_\mathrm{u}/R)\{1-(c_\mathrm{v}^\mathrm{eq}/c_\mathrm{v}) \exp[(p-p_\mathrm{h}-2\gamma/R)\Omega/kT]\}; \quad (3)$$

thus, the capillarity relation, Eq. (1) does not correspond anymore to the quasi-stationary state ($\mathrm{d}R/\mathrm{d}t=0$) if ($c_\mathrm{v}^\mathrm{eq}/c_\mathrm{v}$) $\ll 1$. Moreover, under irradiation conditions the bubble growth is determined also by the diffusion of the non-equilibrium interstitials and the correct expression takes the form [4,5]

$$\mathrm{d}R/\mathrm{d}t = (D_\mathrm{u}/R)\{1-(\beta_\mathrm{i}/\beta_\mathrm{v})-(c_\mathrm{v}^\mathrm{eq}/c_\mathrm{v}) \exp[(p-p_\mathrm{h}-2\gamma/R)\Omega/kT]\}, \quad (4)$$

where $\beta_\mathrm{i}=D_\mathrm{i}c_\mathrm{i}$, $\beta_\mathrm{v}=D_\mathrm{v}c_\mathrm{v}$, D_i and c_i are the interstitial diffusion coefficient and bulk concentration, respectively. This equation can be also rewritten in the form

$$\mathrm{d}x/\mathrm{d}t = D_\mathrm{u}x^{1/3}(3\Omega/4\pi)^{-2/3}(1-\beta_\mathrm{i}/\beta_\mathrm{v})\{1-(c_\mathrm{v}^\mathrm{eq}/c_\mathrm{v}) (1-\beta_\mathrm{i}/\beta_\mathrm{v})^{-1}\exp[(p-p_\mathrm{h}-2\gamma/R)\Omega/kT]\}, \quad (5)$$

where x is the amount of vacancies comprising the void, i.e. $x=(4/3)\pi R^3/\Omega$.

As it will be shown below, at $T<1500$°C the value of ($c_\mathrm{v}/c_\mathrm{v}^\mathrm{eq}$) attains several orders of magnitude (e.g. ($c_\mathrm{v}^\mathrm{eq}/c_\mathrm{v}$) $\approx 10^{-4}$ at $T=1000$°C), whereas $(1-\beta_\mathrm{i}/\beta_\mathrm{v})\approx 10^{-2}$. Therefore, the application of the capillarity relation, Eq. (1) becomes invalid under these conditions, since the quasi-stationary state of a bubble ($\mathrm{d}R/\mathrm{d}t=0$) derived from Eq. (5) corresponds to a new relationship:

$$(p-p_\mathrm{h}-2\gamma/R)\Omega = -kT\ln[(c_\mathrm{v}/c_\mathrm{v}^\mathrm{eq})(1-\beta_\mathrm{i}/\beta_\mathrm{v})]. \quad (6)$$

At 1000°C the difference between $\Delta p=p-p_\mathrm{h}$ and the capillary pressure $2\gamma/R$ is negative (i.e. corresponds to depressurised bubbles) and attains $\approx 10kT/\Omega \approx 10$ GPa, and continues to increase with the temperature decrease (along with the increase of ($c_\mathrm{v}/c_\mathrm{v}^\mathrm{eq}$)).

At $T>1500$°C, as shown below, the radiation-induced concentration c_v really does not exceed the thermal equilibrium value c_v^eq; thus, Eq. (2) becomes valid at high temperatures. However, at $T\leqslant 1500$°C, application of Eq. (4) instead of Eq. (2) for the bubble growth can strongly change the kinetics of the intragranular porosity evolution.

In order to demonstrate this statement, it is sufficient to consider the behaviour of a solely growing bubble during a time interval between two subsequent collisions with other bubbles. It should be noted that the Brownian mobility of bubbles is considered in many theoretical papers to be significant (mainly on the basis of observations [12]), leading to a relatively high frequency of mutual collisions. However, in the subsequent tests [13] it was clearly demonstrated, that at $T\leqslant 1800$°C the Brownian motion of bubbles is negligibly slow, owing to the high facetting of their surface (and/or to the '5-metal particles' attachment invariably observed in large bubbles [14]). Therefore, the time between two subsequent collisions of a bubble (in the absence of temperature gradients in the grain) is really very large. In this case the analysis of the growing bubbles behaviour can be performed on the basis of Eqs. (2) or (5) along with the corresponding kinetic equation for the number of gas atoms N in a bubble:

$$\mathrm{d}N/\mathrm{d}t = 3D_\mathrm{g}c_\mathrm{g}(3\Omega/4\pi)^{-2/3}x^{1/3} \times [1-NK_\mathrm{g}(3\Omega/4\pi)^{2/3}/(3D_\mathrm{g}c_\mathrm{g}x^{1/3})], \quad (7)$$

where D_g and c_g are the gas atom diffusion coefficient and bulk concentration (number of gas atoms per U atom), respectively, K_g is the rate of the radiation-induced resolution of gas atoms from a bubble; and with the Van-der-Waals equation of state:

$$p(x\Omega - bN) = NkT, \quad (8)$$

where $b\approx 8.5\times 10^{-23}$ cm^3/atom is the Van-der-Waals constant for the Xe gas. Since b is very close to 2Ω, in the following consideration Eq. (8) will be represented in the simplified form:

$$p\Omega(x-2N)\approx NkT. \quad (8')$$

For small bubbles, however, the Van-der-Waals approximation might be too rough [15] and a more realistic equation of state (EOS) should be used in the numerical calculations. In the present paper in order to perform analytical calculations and/or estimations, this (Van-der-Waals) approximation will be applied.

It should be noticed, however, that Eq. (7) based on the usual consideration of the gas subsystem in the models [1–3], lacks a term corresponding to the thermal resolution of gas atoms from bubbles. Neglection of such a term is often grounded, however, in many important cases it does not allow a correct description of the system behaviour (in particular, at $T\geqslant 1500$°C, as shown below in Section 4).

2.3. Qualitative analysis of bubble evolution

It is rather illuminating to perform the analysis of the two differential equations (in the simplest case, Eqs. (2) and (7)) in terms of the phase portrait of the system, Fig. 1 (compare with [5, 16]). Intersection of two nodal lines $\mathrm{d}x/\mathrm{d}t=0$ and $\mathrm{d}N/\mathrm{d}t=0$ determines a critical point I of the stable node type, i.e. particles (gas atoms (N) and vacancies (x)) move toward the node from all quadrants in the neighbourhood. In the case of applicability of the ideal gas law (instead of more realistic Eq. (8)) the nodal lines are described by relationships $N\propto x^{2/3}$ and $N\propto x^{1/3}$, respectively. The critical point apparently determines the radius of the stable bubbles and explains the validity of the 'bimodal' bubble size distribution,

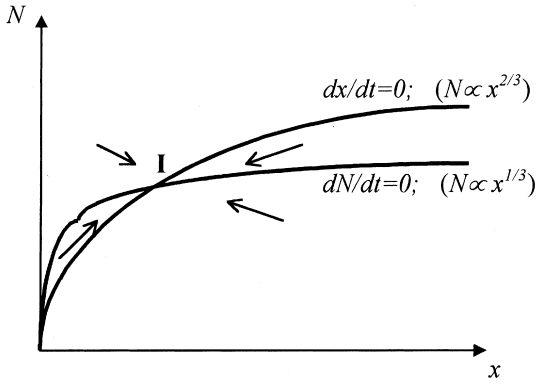

Fig. 1. Schematic diagram of nodal lines in the simplest case of 'capillary' bubble evolution. Velocity vectors and the critical point I (stable node) are indicated. *x*, *N* are amounts of vacancies and gas atoms, respectively, comprising a bubble.

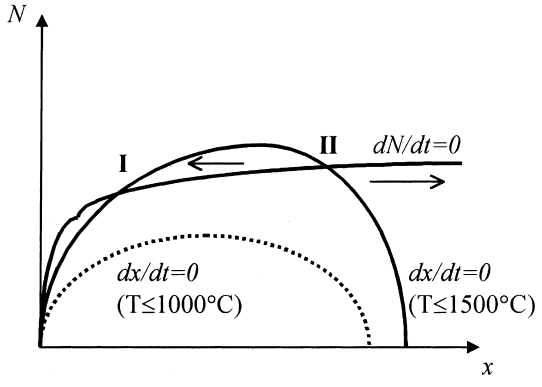

Fig. 2. Nodal lines in the case of non-equilibrium crystal oversaturated with point defects. Two critical points I (stable node) and II (saddle point) are indicated.

observed in the steady-state tests and usually represented by the models based on Eqs. (2) and (7). When a bubble deviates from this stable state, diffusion fluxes of the gas atoms and point defects arise which return the bubble back to the initial state.

For small bubbles with $R < 5$ nm corrections to the ideal gas law become valid, and in the Van-der-Waals approximation for very small bubbles with $R \approx 1$–2 nm the nodal line $dx/dt = 0$ can be satisfactorily described by the limit expression $x = (b/\Omega)N \approx 2N$. In this case the radius of the stable bubble determined by the intersection of the two nodal lines (i.e. the critical point I) is

$$R_I = (6D_g c_g / K_g)^{1/2}. \tag{9}$$

In the case when Eq. (2) is substituted by Eq. (5), the nodal line $dx/dt = 0$ is described by the equation [16]

$$N = [x \ln(S_e) - Ax^{2/3}] / \{(b/\Omega)[\ln(S_e) - Ax^{-1/3}] - 1\}, \tag{10}$$

where $S_e = (c_v / c_v^{eq})(1 - \beta_i/\beta_v)$, $A = (2/3)(36\pi\Omega^2)^{1/3}/kT$, and changes its form with temperature decrease, Fig. 2. At some temperature below 1500°C (i.e. when $S_e > 1$) the second critical point II (of the saddle type) appears which can be reached from the first critical point only due to thermal fluctuations and/or collisions of bubbles. Along with a further temperature decrease the two points approach each other and finally disappear. For the above presented values of the parameters $(c_v^{eq}/c_v) \approx 10^{-4}$ and $[1 - (\beta_i/\beta_v)] \approx 10^{-2}$ attained at $T = 1000$°C, the critical points are knowingly absent, Fig. 3. In this situation bubbles grow unrestrictedly (along the dashed line in Fig. 3). This is generally in contradiction with observations [17–20], which is evidence that the size of bubbles stabilises ($R \approx 0.5$–1 nm) the growth in some

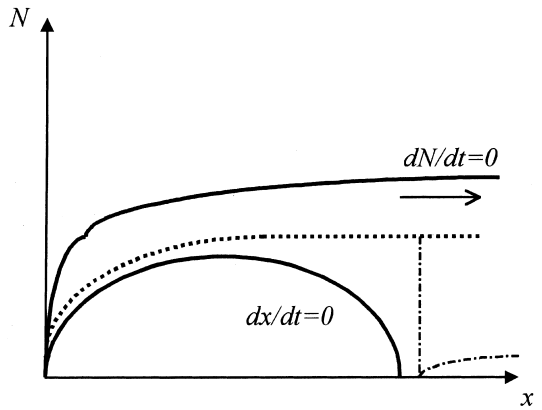

Fig. 3. Nodal lines and trajectory of growing bubbles (dashed line) in the absence of critical points (corresponding to the low temperature case in Fig. 2).

period of time in the reactor steady operation regimes in a wide temperature interval (from 800°C to 1800°C).

2.3.1. Small bubble relaxation mechanism

The main reason for this discrepancy of the theory with observations is apparently connected with an unaccounted additional physical mechanism of bubble interactions with fission fragments. Up to now such interactions were considered only in the equation for the gas subsystem (i.e. Eq. (7)) in the form of the radiation-induced resolution of gas atoms from bubbles. However, one should also take into consideration interactions of fission fragments with the vacancy subsystem which becomes especially important for small bubbles ($R \approx 1$ nm). Indeed, in accordance with the contemporary microscopic theory of the material interactions with high energy fission particles (see, for example, [21]), molten zones appear in the fission fragment tracks during some

short time interval $\tau^* \sim 10^{-11}$ s. Despite the apparent smallness of this time interval, it appears to be large enough for high temperature annealing of a small bubble with $R \approx 1$ nm and its (partial) relaxation to the equilibrium state in the molten zone of the track with diameter $\approx$10 nm. Such a state in the liquid phase is a mechanically equilibrium bubble described by the capillarity relation, Eq. (1), and the relaxation time to this state can be estimated as $\tau_r \sim R/v_s$, where v_s is the sound velocity in the melt. This estimation can be deduced in a similar way to the solution of the problem of an empty void shrinkage in the incompressible liquid [22] by generalisation to the case of a gas filled void, [23]. Assuming $v_s \sim 10^3$ m/s, $R \approx 1$ nm, one gets $\tau_r \sim 10^{-12}$ s $\leqslant \tau^*$.

The simplest way to account for this mechanism is the introduction in Eq. (5) of an additional term, describing bubble relaxation as a result of its collisions with fission fragments. Under the assumption that the path volume V_{tr} is equal to $\pi r_{tr}^2 L$, where $r_{tr} \approx 5$ nm, $L \approx 6 \times 10^{-4}$ cm are the track radius and length, respectively, a mean time between collisions of a small bubble with particles is estimated as $\tau_0 \approx (2V_{tr}F)^{-1} \approx 10^2$ s, where $F \approx 10^{13}$ s^{-1} cm^{-3} is the fission rate [21]. Correspondingly, an additional term $K_v(x - x_L(N))$ is introduced in Eq. (5), where $K_v \propto \tau_0^{-1}$, and $x_L(N)$ corresponds to the capillarity relation expressed in terms of the values x and N. In the considered case of small bubbles with $R \leqslant 1$ nm this relation is completely determined by the Van-der-Waals constant $b \approx 8.5 \times 10^{-23}$ cm^3 and can be reduced to the form $x_L(N) \approx (b/\Omega)N \approx 2N$. A proportionality factor in the relation $K_v \propto \tau_0^{-1}$ may significantly differ from 1 reflecting the probability of incomplete relaxation of a bubble during short-term ($\tau^* \sim 10^{-11}$ s) annealing in the molten zone of a track. Finally, one gets instead of Eq. (5):

$$\begin{aligned} dx/dt = {} & D_u(3\Omega/4\pi)^{2/3}x^{1/3}(1 - \beta_i/\beta_v)\{1 - (c_v^{eq}/c_v) \\ & \times (1 - \beta_i/\beta_v)^{-1}\exp[(p - p_h - 2\gamma/R)\Omega/kT]\} \\ & - K_v(x - x_L(N)). \end{aligned} \quad (11)$$

Analysis of Eq. (11) shows that the additional term in the r.h.s. recreates the critical point at the intersection of the two nodal lines $dx/dt = 0$ and $dN/dt = 0$ and, thus, leads to the stabilisation of the bubble radius in the steady stage of irradiation also in the case of low temperatures (see Fig. 4).

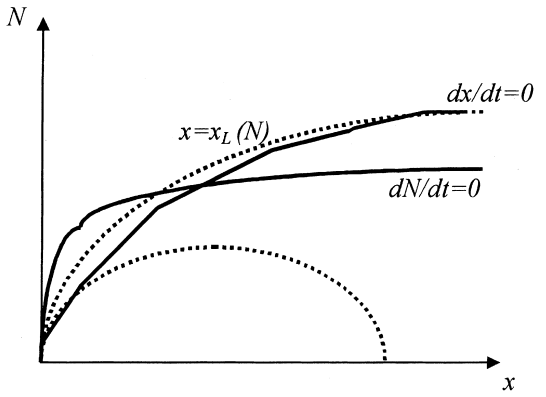

Fig. 4. Nodal lines with account of the small bubble relaxation mechanism (leading to the transformation of Fig. 3).

2.3.2. Large bubble evolution

It should be emphasised, however, that the above proposed mechanism of small bubble annealing becomes invalid for bubbles with a diameter substantially exceeding the width of the fission particle tracks ($2R \gg 10$ nm). Under steady irradiation conditions this limitation is insignificant, since the radii of the bubbles are stabilised and usually do not exceed $\approx$1–2 nm. Under transient conditions the situation can radically change. For example, it was observed in the tests [24] that during a power transient the fuel temperature rises rapidly, leading to the growth of large (10–500 nm diameter) fission gas bubbles. Such large bubbles cannot be annealed in the molten zone of tracks and probably conserve their dimension x or reduce it but essentially less effectively (for example, by the vacancy radiation resolution mechanism similar to the above discussed gas atom resolution from bubbles). In this case the system behaviour is again described by the phase portrait similar to Fig. 3, i.e. large bubbles (with $R \gg 5$ nm) formed during the transient period grow up unrestrictedly, without any preference to the 'capillary' state.

Since in this case (in the absence of restrictions implied by the capillarity relation, Eq. (1)) the gas atom diffusion is not anymore the rate determining step of the bubble growth kinetics, on the one hand, and owing to a relatively small value of the gas atom flux to the growing bubble ($\propto D_g c_g$) in comparison with the effective flux of point defects ($\propto D_u(1-\beta_i/\beta_v)$), on the other hand, bubbles become essentially depressurised and grow up very rapidly (along the dashed line in Fig. 3) in comparison with the usually proposed evolution (along the nodal line $dx/dt = 0$). In particular, this may lead to a significantly larger and quicker swelling of fuel than usually expected.

3. Irradiation effects

Essential factors determining the system behaviour and entering in Eq. (3) are the non-equilibrium point defect concentrations c_v (vacancies) and c_i (interstitials). For their calculation one can use the rate theory continuum model of Brailsford and Bullough [25]:

$$\begin{aligned} dc_v/dt &= K + K_e - D_v c_v k_v^2 - \alpha D_i c_i c_v, \\ dc_i/dt &= K - D_i c_i k_i^2 - \alpha D_i c_i c_v, \end{aligned} \tag{12}$$

where K is the atomic displacement rate, K_e the rate of thermal vacancy production, $k^2_{v(i)}$ the sink strength for vacancies (interstitials), α the recombination constant ($\approx 4\pi r_c/\Omega$, where $r_c \approx 0.1$–0.5 nm). Under PWR reactor normal operation conditions $K = F z_s \Omega$, where F is the fission rate, $z_s \approx (1\text{–}5)\times 10^5$ is the damage formation in the fission track volume, $\Omega \approx 4.1\times 10^{-23}$ cm^3 is the specific volume of the uranium atoms, thus, for the typical value $F = 10^{13}$ cm^{-3} s^{-1}, one can estimate $K \approx 10^{-5}$–10^{-4} s^{-1}.

If voids and dislocations are the only fixed sinks:

$$k_v^2 = 4\pi\rho_b R + Z_v\rho_d, \quad k_i^2 = 4\pi\rho_b R + Z_i\rho_d, \tag{13}$$

where ρ_b and ρ_d are the void number and dislocation density, respectively; the dislocation sink strength constants Z_v and Z_i for vacancies and interstitials are of the order of unity, but Z_i is a few percent larger due to the higher elastic interaction between dislocations and interstitials, than with vacancies.

For the calculation of the bulk concentrations c_v and c_i, the grain boundary sink strength $k^2_{g.b.}$ can be neglected in comparison with the bulk sinks $k^2_{v,i}$ (after some initial irradiation period when $k^2_{v,i}$ becomes $>10^{10}$ cm^{-2}), since

$$k^2_{g.b.}/k^2_{v,i} \approx 3/(R_g k_{v,i}) \ll 1,$$

where R_g is the grain radius [25].

In the steady state ($dc_v/dt = dc_i/dt = 0$) the general solution of Eqs. (12) is

$$\begin{aligned} c_i &= (D_v k_v^2/2D_i\alpha)[-(1+\mu) + ((1+\mu)^2 + \eta)^{1/2}], \\ c_v &= (k_i^2/2\alpha)[-(1-\mu) + ((1+\mu)^2 + \eta)^{1/2}], \end{aligned} \tag{14}$$

where

$$\eta = 4\alpha K/(D_v k_i^2 k_v^2), \quad \mu = K_e\eta/(4K) \tag{14'}$$

3.1. Low temperatures, $T \leqslant 1500$°C

A $T \leqslant 1500$°C, $K_e \ll K$; as it will be demonstrated below. On the other hand, η occurs to be rather large ($\gg 1$) during a very long initial stage of the steady-state period of irradiation. Indeed, at $T \approx 1000$°C $D_v \approx 10^{-11}$–10^{-12} cm^2/s (see Eq. (18) and/or compare with data presented in [26]), and the relationship $\eta \gg 1$ is valid until the parameters k_i^2, k_v^2 attain the value $\approx 10^{11}$–10^{12} cm^{-2}, i.e. practically up to the maximal observed number density of the bubbles (with $R \approx 1$ nm), $\rho_b \approx 10^{17}$–10^{18} cm^{-3}. At higher temperatures (up to 1500°C) this relationship is valid in a slightly reduced range of the parameter $k^2_{v,i}$ variation owing to some possible increase (within one order magnitude, [26]) of D_v. At lower temperatures (below 1000°C) the uranium self-diffusion coefficient D_u becomes completely athermal and independent of temperature:

$$D_u \approx AF,$$

where $A \approx 1.2\times 10^{-29}$ cm^5 [25,26]; thus, $D_u \approx 10^{-16}$ cm^2/s at the fission rate $F \approx 10^{13}$ cm^{-3} s^{-1}. As shown below (Eq. (18)), D_v becomes also temperature independent and, thus, the applicability range of the relationship $\eta \gg 1$ does not reduce. This is a rather important conclusion, since in this case the general solution, Eq. (14) can be radically simplified:

$$c_v \approx (K\Omega k_i^4/4\pi r_c k_v^2 k_i^2 D_v)^{1/2} \approx (K\Omega/4\pi r_c D_v)^{1/2}, \tag{15}$$

$$D_i c_i \approx D_v c_v (k_v^2/k_i^2), \tag{16}$$

i.e. c_v, c_i become practically independent of the amount of voids and dislocations in the crystal, since the mutual recombination of the point defects dominates in this stage. Owing to $D_u \approx D_v c_v \approx D_i c_i$, finally one gets

$$c_v \approx K\Omega/4\pi r_c D_u, \tag{17}$$

$$D_v \approx 4\pi r_c D_u^2/K\Omega. \tag{18}$$

Correspondingly, at $T \leqslant 1000$°C ($D_u \approx 10^{-16}$ cm^2/s) one gets $c_v \approx 10^{-5}$, $D_v \approx 10^{-11}$ cm^2/s. At higher temperatures (up to 1500°C), D_u increases slowly up to its thermal value at 1500–1600°C, $D_u \approx 10^{-15}$ cm^2/s. Therefore, the calculated value of c_v reduces to $\approx 10^{-6}$, i.e. c_v attains its equilibrium value at ≈ 1500°C, $c_v^{eq} \approx \exp(-2.2\ \text{eV}/kT) \approx 6\times 10^{-7}$ [26].

3.1.1. Nucleation factor

It is important to notice that Eq. (17) allows the calculation of the so-called nucleation factor F_N, introduced in many models as a default value (usually varying in a wide range 10^{-4}–10^{-7}) to determine the probability that two gas atoms that have come together actually stick and form a bubble [1–3]. It is easy to understand that for the stability of such a bubble at least one vacancy must be located in the position of the two atoms collision; otherwise, the formed bubble will immediately disintegrate. This can be demonstrated if one formally extends the bubble state equation, Eq. (8), to small bubbles with $N = 2$. Indeed, it is generally accepted now that gas atoms diffuse in neutral trivacancies (i.e. clusters of a U vacancy and two O vacancies), or charged trivacancies (i.e. clusters of two U vacancies and one O vacancy), rather than in single vacancies [25,26]. In the first case (neutral trivacancies) at least three additional U vacancies are necessary to form after collision a stable bubble obeying a restriction of Eq. (8): $x/N \geqslant b/\Omega > 2$. Such an event has a very low probability proportional to c_v^3. However, in the second case (charged trivacancies) only one additional vacancy is necessary.

The probability that a vacancy is located in a certain position (of a two atoms collision) is exactly equal to the vacancy bulk concentration c_v. In this case the nucleation factor can be deduced from Eq. (17):

$$F_N = c_v \approx K\Omega/4\pi r_c D_u. \quad (19)$$

Therefore, at $T \leqslant 1000$°C

$$F_N \approx z_s \Omega^2/4\pi r_c A,$$

or

$$F_N \approx 10^{-5} - 10^{-4}, \quad (20)$$

and at higher temperatures (up to 1500°C) F_N smoothly reduces within one order of magnitude (along with the possible increase of D_u):

$$F_N \approx 10^{-6} - 10^{-5}. \quad (21)$$

These values are in reasonable agreement with the default value $F_N \approx 10^{-4}$–10^{-7} accepted in Refs. [1–3]. Hence, this result can be considered as an indirect confirmation of the charged trivacancy diffusion mechanism of gas atoms in UO_2 at high temperatures.

Above 1500°C the thermal equilibrium concentration c_v^{eq} should be used for evaluation of the nucleation factor:

$$F_N \approx c_v^{eq} \approx \exp(-2.2\ \mathrm{eV/kT}). \quad (22)$$

It should be kept in mind, however, that the obtained results for the nucleation factor F_N are valid until the critical nucleus size is small in comparison with the minimal bubble size, $R_{cr} = 2\gamma/(c_g P_s/c_s) < (3\Omega/\pi)^{1/3}$ (see Section 4.2). Otherwise, the correct description should be based on the calculation of the activation barrier for the fluctuation formation of the critical nucleus (see Section 4.3). Thus, Eqs. (20)–(22) are valid only in a certain gas concentration range, attained during various periods of irradiation (e.g. under steady irradiation conditions they are not valid during some initial ('incubation') period at each temperature and during a late stage period at high temperatures, see Section 4.3).

3.1.2. Sink strengths

In order to calculate the parameter $(1-\beta_i/\beta_v)$ at $T < 1500$°C which at these temperatures is equal to $1-(k_v^2/k_i^2)$ (see Eq. (16)) and, thus, becomes a small value ($\ll 1$), one should take into account that in this case an additional problem of calculation of the dislocation density ρ_d (determination of the dislocation sink strength $Z_{i,v}\rho_d$) arises. In the initial stage of irradiation, when the bubble number density ρ_b is low while the dislocation density is finite and determined by the original state of the crystal (usually estimated as $\rho_d \approx 10^8$ cm^{-2}), $4\pi\rho_b R \ll Z_{i,v}\rho_d$; therefore, one gets $k_i^2 \approx Z_i\rho_d$, $k_v^2 \approx Z_v\rho_d$, and $1 - \beta_i/\beta_v \approx 1 - Z_v/Z_i \approx 10^{-2}$ from Eq. (13).

Along with the irradiation dose increase, the bubble number density ρ_b and dislocation density ρ_d simultaneously increase. While the bubble sink strength $4\pi\rho_b R$ does not exceed the dislocation sink strength $Z_{i,v}\rho_d$, the value $1 - \beta_i/\beta_v$ remains the same. From the analysis of the equation for the radius R_L of the growing interstitial dislocation loops (with the Burgers vector b) [28]

$$dR_L/dt \approx b^1(Z_i D_i c_i - Z_v D_v c_v) \approx b^{-1} Z_v D_v c_v [(Z_i/Z_v)(k_v^2/k_i^2) - 1],$$

it is straightforward to see that while $4\pi\rho_b R \ll Z_{i,v}\rho_d$ is valid (i.e. $k_i^2 \approx Z_i\rho_d$, $k_v^2 \approx Z_v\rho_d$), the dislocation loop growth is strongly suppressed (with respect to the bubble growth):

$$dR_L/dt \propto [(Z_i/Z_v)(Z_v/Z_i) - 1] \to 0.$$

In the opposite case of a large number density of bubbles, $4\pi\rho_b R \gg Z_{i,v}\rho_d$, and $k_i^2 \approx k_v^2 \approx 4\pi\rho_b R$, the bubble growth turns to be suppressed (with respect to the loop growth), since from the equation for the growing bubble radius:

$$dR/dt \approx R^{-1}(D_v c_v - D_i c_i);$$

in this case one can deduce

$$dR/dt \approx R^{-1} D_v c_v (1 - k_v^2/k_i^2) \to 0.$$

Therefore, it is logical to assume that after some time the relationship $4\pi\rho_b R \approx Z_{i,v}\rho_d$ becomes valid, and the further growth of the bubbles and dislocation loops occurs self-consistently, in accordance with this relationship. In this case $1 - \beta_i/\beta_v$ remains $\approx 10^{-2}$. Indeed, this conclusion can be selectively confirmed by some data found in the literature. For instance, in the tests [24] both densities ρ_b and ρ_d were measured after some period of the steady irradiation: $\rho_b \approx 10^{16}$ cm^{-3}, $\rho_d \approx 10^{10}$ cm^{-2}, and the mean bubble radius $R \approx 4$ nm, thus, the approximate equation $4\pi\rho_b R \approx Z_{i,v}\rho_d$ was really valid.

After completion of the 'recombination stage', $\eta \leqslant 1$ and dislocations and bubbles become the main sinks determining the steady-state concentration of the point defects, i.e. Eqs. (15) and (16) become invalid. As already mentioned, at $T \leqslant 1500$°C the transition to the new regime occurs at a late stage of the steady irradiation, when the bubble number density attains $\rho_b \approx 10^{17}$–10^{18} cm^{-3}. In the new regime the general steady-state solution Eq. (14) can be reduced to the form

$$c_v \approx K/k_v^2 D_v, \quad \text{or} \quad K \approx k_v^2 D_v c_v \approx k_v^2 D_u.$$

As already mentioned, at $T \leqslant 1000$°C D_u depends only on the fission rate F and does not depend on temperature. At higher temperatures (up to 1500°C) D_u smoothly increases within one order of magnitude. Therefore, in the new regime k_v^2 attains the steady value:

$$k_v^2 \approx K/D_u \approx z_s\Omega/A. \quad (23)$$

This value depends weakly on temperature, being $k_v^2 \approx 10^{11}$–10^{12} cm^{-2} at $T \leqslant 1000$°C and possibly reducing within one order of magnitude at $T \leqslant 1500$°C. Moreover, in all these cases k_v^2 corresponds to the maximum value attained in the recombination stage (see Section 3.1). Indeed, after substitution of Eq. (18) in Eq. (14') one can see that the value $k_v^2 = K/D_u$ calculated in Eq. (23) determines the upper limit of the recombination stage providing $\eta = 1$.

This means that the maximum value of k_v^2 attained at $T \leqslant 1500$°C in the recombination stage is practically final and does not increase anymore during the subsequent stage. Since $k_{v,i}^2 = 4\pi\rho_b R + Z_{v,i}\rho_d$, and, as shown above, $4\pi\rho_b R \approx Z_{i,v}\rho_d$, then the attained stabilised value of the bubble number density is $\rho_b \approx 10^{17}$–10^{18} cm^{-3} (for the bubbles with $R \approx 0.5$–1 nm), in a fair agreement with experimental data for the number density observed under steady irradiation conditions [17–20]. Thus, using the most recent and reliable data [20] one can evaluate $4\pi\rho_b R \approx 6\times10^{11}$ cm^{-2} in a wide temperature range 900–1700°C.

3.1.3. Bubble system stabilisation

In order to evaluate a relationship between the values k_v^2 and R in the stage of the bubble system stabilisation, an additional consideration of the gas atom conservation should be carried out. In this stage all generated gas atoms diffuse to the grain boundaries (without being captured by the stabilised, or 'saturated' intragranular bubble system), thus the balance equation takes the form

$$G\Omega = k_{g.b.}^2 D_g c_g,$$

where $G = \beta F$, $\beta \approx 0.25$ is the number of gas atoms generated per one fission, $k_{g.b.}^2 \approx 3k_v/R_{gr}$ an approximate expression for the sink strength of the grain boundary (under condition $k_v^2 \gg k_{g.b.}^2$) [25], $R_{gr} \approx 5$ μm the grain radius. Using Eq. (9) for the bubble radius, $R_I = (6D_g c_g/K_g)^{1/2}$, one gets a relationship for the radius R_{st} of the stabilised bubbles:

$$R_{st} = (6D_g c_g/K_g)^{1/2} \approx (2\beta\Omega R_{gr}/b_0 k_v)^{1/2}, \quad (24)$$

where $b_0 = K_g/F$ is assumed $\approx 10^{-18}$–10^{-17} cm^3 [29,30]. Thus, with temperature increase from 1000°C to 1500°C the bubble radius slightly increases by a factor 1.5–1.8 (along with a k_v^2 decrease within one order of magnitude), 0.6 nm $\leqslant R_{st} \leqslant$ 1 nm, in reasonable agreement with observations (e.g. [20]). Since $k_v^2 \approx 4\pi R_{st}\rho_b$, for the total volume of bubbles V_b (per cm^3) one gets

$$V_b = 4\pi R_{st}^3 \rho_b/3 \approx 2\beta\Omega R_{gr} k_v/3b_0.$$

The stabilised volume calculated in this equation corresponds to the total amount (per cm^3) of the gas atoms in the bubbles $c_b \approx V_b/b \approx V_b/2\Omega$:

$$c_b \approx \beta R_{gr} k_v/3b_0 \approx 10^{19} \text{ atoms/cm}^3, \quad (25)$$

in reasonable agreement with the measurements [19,20,31]. In these tests performed in a wide temperature interval 1000–1700°C and various burnups exceeding 2×10^{20} fissions/cm^3, the total amount of gas atoms in bubbles was $\approx(1$–$3)\times10^{19}$ cm^{-3} and the radius of bubbles was ≈0.6–1 nm.

It is interesting to note that this result can be used for independent evaluation of the radiation resolution factor b_0. Using the experimentally measured value $c_b \approx (1$–$3)\times10^{19}$ atoms/cm^3, one obtains from Eq. (25)

$$b_0 \approx \beta R_{gr} k_v/3c_b \approx 10^{-18}\text{–}10^{-17} \text{ cm}^3, \quad (26)$$

in the above indicated measured temperature and irradiation ranges, that is in a reasonable agreement with more direct (but relatively rough and performed for large bubbles $R \leqslant$ 5–7 nm) measurements of $K_g = Fb_0$ in [29], $K_g \approx 10^{-5}$–10^{-4} s^{-1}.

The estimation of b_0 obtained in Eq. (26) can be also justified by the following consideration. In the tests [20] with a burnup of 2×10^{20} fissions/cm^3, the gas concentration in the matrix did not exceed the total generated value 5×10^{19} cm^{-3}, i.e. $c_g \leqslant 2\times10^{-3}$, Thus, using the first part of Eq. (24) for the 1000°C test (in which $R_{st} \approx$ 0.5–0.6 nm and $D_g \approx 8\times10^{-17}$ cm^2/s [32]), one deduces the upper limit for the radiation resolution rate, $K_g \leqslant 3.2\times10^{-4}$ (or $b_0 \leqslant 3.2\times10^{-17}$ cm^3, if $F = 10^{13}$ fissions/(cm^3 s)). At such a low temperature c_g was really very close to the total generated value 5×10^{19} cm^{-3}, since c_b was evaluated in [20] as $\approx 1\times10^{19}$ atoms/cm^3 (i.e. only ≈20%) and the gas content in the intergranular bubbles is even smaller (10–15%) at this temperature [33]; thus, the calculated upper limit $K_g \approx (2$–$3)\times10^{-4}$ s^{-1} should be very close to the real value.

This value practically coincides with the latest measurements [30] and can be further used for the evaluation of $D_g c_g$ from the experimental data [19,20,31] for the bubble radius:

$$D_g c_g = R_{st}^2 K_g/6 \approx (2-5)\times10^{-19} \text{ cm}^2/\text{s}. \quad (27)$$

This equation determines the stabilised value of c_g, if one uses data for D_g from [32], which are generally accepted and well confirmed (for example, by recent measurements [34]), see Table 1.

3.2. High temperatures, $T \geqslant 1500$°C

At $T \geqslant 1500$°C the thermal effects dominate over the radiation ones, $K_e \geqslant K$, and the general solution, Eq. (14), self-consistently transforms into

$$\begin{aligned} &c_v \approx K_e/k_v^2 D_v \approx c_v^{eq}, \\ &D_i c_i \approx D_v c_v (k_v^2/k_i^2)(K/K_e) \ll D_v c_v; \end{aligned} \quad (28)$$

therefore, $1 - \beta_i/\beta_v = 1 - (D_i c_i/D_v c_v) \approx 1$.

Table 1
The single gas atom diffusion coefficient in UO_2 under irradiation, $F \approx 10^{13}$ fissions/(cm^3 s) (after Turnbull [31])

T (°C)	800	1000	1100	1200	1300	1400	1500	1600	1700
D_g (cm^2/s)	2×10^{-17}	8×10^{-17}	1.5×10^{-16}	4.5×10^{-16}	1.7×10^{-15}	6.3×10^{-15}	2×10^{-14}	5.8×10^{-14}	3.8×10^{-13}

In contrast with the low temperature case, Eq. (28) does not imply any limitations to the value of k_v^2. Therefore, additional (thermal) mechanisms should be considered in order to explain the observed stabilisation of this parameter at high temperatures.

4. Thermal effects

As already mentioned in Section 2.2, an additional term representing the thermal resolution of gas atoms from bubbles is usually not considered in the equation describing the behaviour of the gas subsystem, Eq. (7) [1–3]. It will be demonstrated here, however, that at high temperatures namely such a process determines the mechanism of bubble nucleation, becomes responsible for the observed stabilisation of the bubble number density at a late stage of steady irradiation and significantly influences the gas system behaviour during high temperature annealing of irradiated fuel.

4.1. Thermal resolution of gas atoms from bubbles

In the Van-der-Waals approximation the account of the thermal resolution of gas atoms from a bubble transforms Eq. (7) into the following one:

$$\begin{aligned} dN/dt = {} & 3D_g c_g (3\Omega/4\pi)^{-2/3} x^{1/3} \\ & \times [1 - (3\Omega/4\pi)^{2/3} NK_g/(3D_g c_g x^{1/3}) \\ & - (p/p_e)\exp(b(p-p_e)/kT)], \end{aligned} \tag{29}$$

where $p = kTN/\Omega(x-2N)$ is the bubble pressure ($p \gg p_h$) and p_e the partial gas pressure in equilibrium with the solid solution of gas atoms in the fuel matrix, which determines the critical nucleus radius $R_{cr} = 2\gamma/p_e$. Assuming Henry's law behaviour up to the terminal solubility c_s, one gets $p_e = (p_s/c_s)c_g$. However, the ratio (p_s/c_s) is unknown, thus, it can be only roughly evaluated from the available indirect data. It is known from the literature [35] that the solubility of He in UO_2 measured in the pressure range 5–10 MPa at 1200°C, yields $(p_s/c_s) \approx 1.5\times10^{12}$ Pa. On the other hand, for the fission gas (Xe and Kr) it can be evaluated on the base of observations [36] that under steady irradiation conditions at $T = 1200$°C visible bubbles appeared at burnup of $\approx 3\times10^{19}$ fissions/cm^3, which corresponded to the gas concentration $\tilde{c}_g \approx 3\times10^{-4}$. Assuming that a bubble formed due to sticking of two atoms (see Section 3.1.1) and continues to grow up if its radius $R = (3\Omega/\pi)^{1/3}$ exceeds the critical nucleus radius R_{cr}, one gets an estimation at $T = 1200$°C: $(p_s/c_s) \approx 3\times10^{13}$ Pa. This value will be used hereafter for quantitative estimations, bearing in mind that it can increase with temperature in accordance with the Arrhenius law. A similar conclusion about the existence of the critical nucleus size associated with the observed threshold value of the gas concentration, was derived in Ref. [31].

4.2. Bubble system stabilisation at high temperatures

It is clearly seen that when the second (irradiation) term in Eq. (29) dominates over the third (thermal) one, the steady solution $dN/dt = 0$ determines the critical point I, calculated in Eq. (9) and stabilised under the condition of Eq. (27), $D_g c_g = R_{st}^2 K_g/6$. On the other hand, when the third term dominates over the second one, the steady solution determines the critical nucleus size: $R_{cr} = 2\gamma/(c_g p_s/c_s)$. At temperatures 800–1000°C ($D_g \approx (2\text{–}8)\times10^{-17}$ cm^2/s [32], $R_{st} \approx 0.5$–0.6 nm [18,20]) the value of c_g attained under the stabilisation condition, Eq. (27) is rather high, $c_g^* \approx 10^{-3}$–10^{-2} and corresponds to a very small value of $R_{cr}^* \leqslant 0.1$ nm. This means that at low temperatures the irradiation induced resolution always dominates over the thermal one. However, with the temperature increase the value c_g^* decreases, leading to the increase of the critical nucleus size R_{cr}^* in the stabilised state. Coincidence of the two radii $R_I^* \approx R_{cr}^* \approx 1$ nm occurs (assuming $K_g \approx (1\text{–}3)\times10^{-4}$ s^{-1}, $(p_s/c_s) \approx 3\times10^{13}$ Pa) when $D_g \approx (0.3\text{–}1)\times10^{-14}$ cm^2/s, i.e. at $T \approx$ 1400–1500°C. At $T \geqslant 1500$°C, when the saturation condition, Eq. (23), is not anymore valid, the bubble system stabilisation occurs under the condition $R_I \approx R_{cr}$, which determines the value of the attained concentration $c_g \approx (2\gamma^2 K_g c_s^2/3p_s^2 D_g)^{1/3}$ and corresponding radius $R \approx (12\gamma D_g c_s/p_s K_g)^{1/3}$.

With the temperature increase from 1500°C to 1700°C the diffusion coefficient D_g increases approximately by one order of magnitude, leading to the critical bubble radius increase $R_{cr} \propto D_g^{1/3}$ by a factor of 2. In reality the observed increase of the bubble radius is somewhat smaller (≈1.3–1.5 times) [20]; this apparently can be explained by the unaccounted Arrhenius dependence of the factor (p_s/c_s) on temperature in Henry's law for the solid solute of gas atoms.

In terms of the system phase portrait (see Section 2.3), the above described qualitative consideration can be presented in the following way. As soon as the critical nucleus size exceeds the interatomic distance, a new critical point III (of the saddle type) appears at the intersection of the two nodal lines, Fig. 5. With further

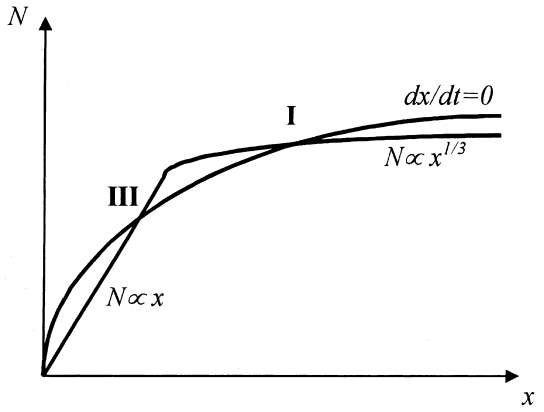

Fig. 5. Nodal lines in the high temperature case ($T \geqslant 1500$°C) with account of the thermal resolution of gas atoms from bubbles. Saddle point III corresponds to the critical nucleus.

decrease of c_g the critical point approaches to the other intersection point I (which determines the steady size of bubbles), and finally coincides with this point, Fig. 6. This situation corresponds to the final state of the bubble system evolution, stabilised with respect to both the bubble size and density number under steady irradiation conditions.

Indeed, since the range of the bubble size growth (between points III and I in Fig. 5) reduces to zero (Fig. 6), the bubble radius is completely stabilised. Since this radius corresponds to the critical nucleus, on the one hand, and significantly exceeds the interatomic distance, on the other hand, the probability of new bubbles generation at this stage is exponentially small. Moreover, if one assumes that new bubbles nevertheless appear after some long period of time, the subsequent reduction of the gas atom concentration c_g leads to the separation of the nodal lines (dashed line in Fig. 6) and to the disappearance of the critical point (i.e. the critical nucleus size). In its turn, this immediately leads to the initiation of the bubbles resolution, the c_g increase, and the recreation of the stabilised state of the system. It is worthwhile to note that such a state is rather similar to the state described by the Lifshitz–Slyozov point in the theory of the late stage precipitation and thermal coarsening in solid solutes [37]. Therefore, the given quasi-stationary state is stable and corresponds to a late stage of steady irradiation when all the generated fission gas atoms diffuse to the grain boundaries without capture by the stabilised (with respect to the bubble size and number) system of the intergranular bubbles.

Exact numerical calculations of the two nodal lines (in the Van-der-Waals approximation for gas atoms in bubbles) are presented in Figs. 7–10 and completely confirm the above presented qualitative consideration (based on the ideal gas law) illustrated in Figs. 5 and 6.

4.3. Bubble nucleation mechanism at high temperatures

As indicated above, nucleation of bubbles is observed only at a relatively high gas concentration $\tilde{c}_g \approx 3\times10^{-4}$, when the critical nucleus size $R_{cr} = 2\gamma/(c_g p_s/c_s)$ becomes less than the minimum stable bubble ($N=2$) size $R=(3\Omega/\pi)^{1/3}$. At 1400°C this value $\tilde{c}_g \approx 3\times10^{-4}$ (attained after $\approx 10^6$ s of irradiation) exceeds the stabilised value $c_g^* \approx 3\times10^{-5}$ attained later (after 10^7–10^8 s) and determined by Eq. (27). This means that after $\approx10^5$ s of irradiation (when the final concentration $\approx3\times10^{-5}$ was initially reached) bubbles were unable to nucleate (since the critical nucleus radius was too large, $R_{cr} \approx 1$ nm) and the gas concentration continued to increase until the critical nucleus size was reduced to $(3\Omega/\pi)^{1/3} \approx 0.3$ nm. There upon the gas concentration in the matrix began to fall down owing to nucleation and growth of bubbles,

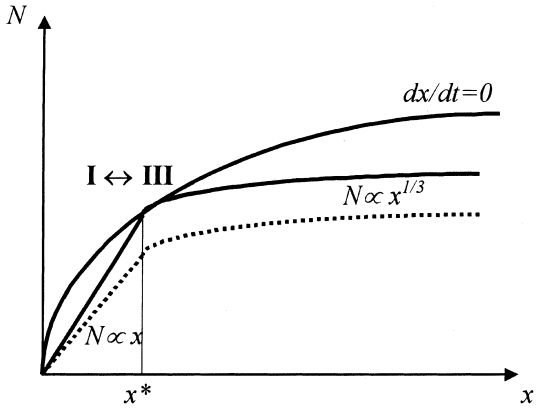

Fig. 6. Nodal lines in the case of the two critical points I and III coincidence, corresponding to stabilisation of bubble size and number under steady state irradiation conditions at $T \geqslant 1500$°C.

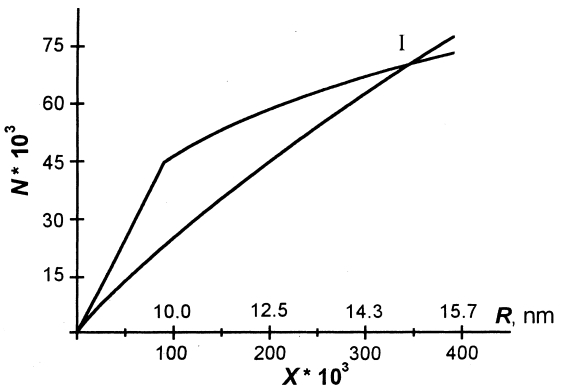

Fig. 7. Numerical calculation of the two nodal lines and one critical point I at $T \approx 1500$°C and high gas atom concentration, $c_g = 10^{-3}$ (other parameters: $D_g = 10^{-14}$ cm^2/s, $K_g = 10^{-5}$ s^{-1}).

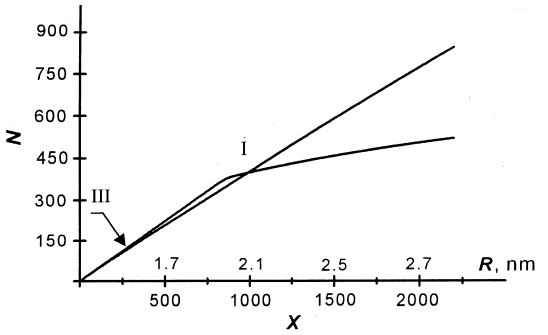

Fig. 8. Numerical calculation of the two nodal lines and two critical points I and III at $T \approx 1500$°C and $c_g = 4\times10^{-5}$ (other parameters: $D_g = 10^{-14}$ cm^2/s, $K_g = 10^{-5}$ s^{-1}).

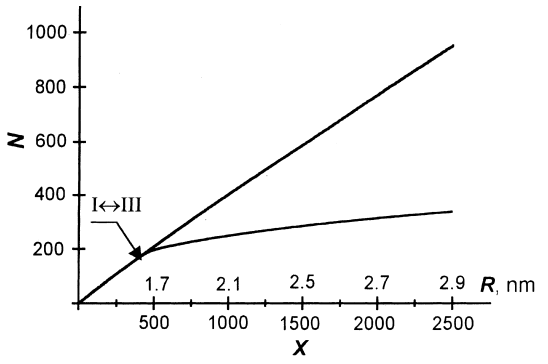

Fig. 9. Numerical calculation of the two nodal lines and two coinciding critical points I and III at $T \approx 1500$°C and $c_g = 2.5\times10^{-5}$, corresponding to the bubble system stabilisation (other parameters: $D_g = 10^{-14}$ cm^2/s, $K_g = 10^{-5}$ s^{-1}).

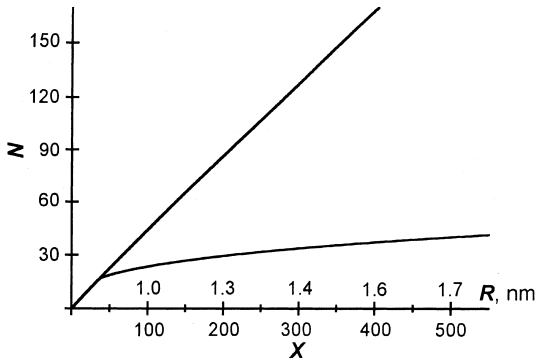

Fig. 10. Numerical calculation of the nodal lines and critical points at $T \approx 1500$°C: the same as Fig. 9, but $K_g = 10^{-4}$ s^{-1} and $c_g = 5\times10^{-5}$.

until the stabilised value c_g* was finally attained. Such a behaviour at high temperatures (with somewhat decreasing $\tilde{c}_g = 2\gamma(\pi/3\Omega)^{1/3}(p_s/c_s)^{-1}$, owing to the Arrhenius dependence of p_s/c_s on temperature) differs qualitatively

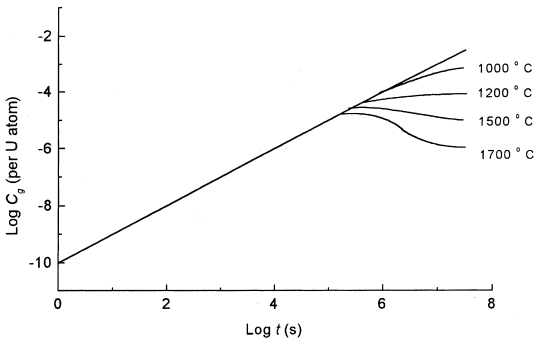

Fig. 11. Schematic representation of the concentration c_g evolution with time under steady irradiation at various temperatures.

from that at lower temperatures (see Fig. 11), since at $T < 1200$°C the gas concentration in the matrix monotonously increases up to the finally stabilised value (which is $\geqslant 3\times10^{-4}$, according to Eq. (27)), corresponding to a small critical nucleus size, $R_{cr} \ll 0.3$ nm.

For this reason, at high temperatures in the stage of the gas concentration decrease, bubble nucleation occurs with some activation energy according to the Volmer–Zeldovich mechanism [37]. Correspondingly, the bubble nucleation process at $T > 1200$°C becomes more heterogeneous with the temperature increase and can be associated with the increased efficiency of fission particle tracks as probable nucleation sites. This is in accordance with electron microscopy observations [20,31] of the increasing amount of bubbles on tracks with temperature (from ≈10% at 1500°C [31] up to ≈100% at 1800°C [20]).

Naturally, under conditions of a finite size of the critical nucleus the description of the bubble formation by the constant nucleation factor F_N (considered in Section 3.1.1) becomes invalid, and the correct description has to be based on the calculation of the activation barrier E_a for the fluctuation formation of the critical nucleus, $F_N \propto \exp(-E_a/kT)$.

4.4. Thermal coarsening of bubbles during post-irradiation annealing

A relatively rapid growth of the intragranular bubbles owing to the gas atom diffusion from the solid matrix is usually observed during high temperature annealing of irradiated fuel [29,33]. A noticeable decrease (by several orders of magnitude) of the bubble number density occurs simultaneously with the bubble size increase. This process of the bubble number decrease in the currently existing models (codes) is usually associated with the Brownian motion of the bubbles leading to their coagulation (via direct collisions) into larger ones in the grain bulk and transport to the grain boundaries. However, even a simple evaluation of the

experimental data shows that a rather low mobility of the bubbles at $T \leqslant 1800$°C measured in [13] does not allow a correct description of the bubble sizes and number densities observed in the annealing stage. For this reason, additional mechanisms of the bubble diffusivity increase under annealing conditions should be invoked (and will be published elsewhere). A complementary mechanism of the bubble growth under annealing conditions can be associated with the thermal effects, discussed in the current Section 4 and generally unaccounted in the standard analysis of the bubble system behaviour.

Indeed, in the absence of irradiation ($K \to 0$ in Eq. (12)), the subsystem of point defects (vacancies and interstitials) attains rather quickly its equilibrium state ($c_{v,i} = c_{v,i}^{eq}$) in the annealing stage. This relaxation time at the annealing temperature 1500°C can be estimated from Eq. (12) as $\tau_{eq} \approx (D_v k_v^2)^{-1} \approx 10^{-1}$–$10^{-2}$ s, where $D_v \approx 10^{-9}$–10^{-10} cm^2/s is the thermal value of the vacancy diffusion coefficient [26]. A slower process of bubble growth occurs owing to the gas atom and point defect diffusion transport to bubbles. Since $D_g c_g \ll D_u$, where $D_u \approx 10^{-16}$–10^{-15} cm^2/s is the thermal value of the uranium self-diffusion coefficient, the gas transport determines the bubble growth rate during the annealing stage. During this growth, extended defects such as dislocation loops, grain boundaries, etc. serve as sources for vacancies (necessary for the bubble growth) and afford the equilibrium concentration of the point defects in the crystal bulk. This may explain the observed dislocation creep and enhanced bubble growth by dislocation sweeping under annealing conditions [17]. Despite a relative slowness of this process (in comparison with thermalisation of point defects), sinking of gas atoms into bubbles may occur during a few minutes or seconds at high temperatures. Hence, under conditions of the tests [29,33], in which fuel samples irradiated at $T \approx 900$°C [33] and 700°C [29] to a burnup of $\approx 2 \times 10^{20}$ fissions/cm^3 were annealed at $T = 1500$°C during 5 h, the characteristic time τ_s of diffusional sinking of gas atoms into bubbles is estimated as $\tau_s \approx (D_g k_v^2)^{-1} \approx 10^2$ s.

Neglecting the thermal resolution term in Eq. (27), one obtains that the gas atom concentration c_g falls down practically to zero during the time interval $\leqslant 10^3$ s of the annealing stage. In reality, however, the critical nucleus radius $R_{cr} = 2\gamma/[c_g(p_s/c_s)]$ increases along with c_g decrease and attains the mean value of the bubble radius $\overline{R}$ at some small but finite value of c_g ($\approx 10^{-5}$ according to estimations in Section 4.2). There upon the rapid diffusion sinking of gas atoms into bubbles ceases and a slower process of the bubble thermal coarsening (Ostwald ripening) commences. This process is qualitatively equivalent to the late stage precipitation in solid solutes described by the Lifshitz–Slyozov theory [37] and corresponds to a slow growth of the 'supercritical' bubbles ($R \geqslant R_{cr}$) and dissolution of 'subcritical' bubbles ($R \leqslant R_{cr}$), affording a simultaneous increase of the mean bubble radius $\overline{R}$ and the critical radius R_{cr} with $R_{cr} \approx \overline{R}$.

It should be emphasised that the analogy between the considered case of the bubbles growth and the Lifshitz–Slyozov model turns to be very close until bubbles are sufficiently small. Indeed, small bubbles with $R \ll 5$ nm are strongly pressurised and thus satisfactorily described by the high-pressure limit expression for the Van-der-Waals gas: $\Omega_g \approx b$, where Ω_g is the specific volume of gas atoms in a bubble, $b \approx 2\Omega$ is the Van-der-Waals constant (see Eq. (8)). For this reason, the diffusional growth of a small bubble is described by the equation

$$dR/dt \approx D_g c_g b(R - R_{cr})/R^2 = (2D_g/R)(\Delta - \sigma/R), \quad (30)$$

where $\Delta = (b/2\Omega)c_g \approx c_g$, $\sigma = (b/2\Omega)c_g R_{cr} \approx c_g R_{cr} = 2\gamma(p_s/c_s)^{-1}$. This equation is similar to the corresponding equation in the Lifshitz–Slyozov theory, allowing direct application of these theoretical results to the considered case of the small bubbles growth.

However, it should be taken into consideration that for larger bubbles, $R \approx 5$ nm, the gas state equation, Eq. (8), is more complicated and the bubble growth equation, Eq. (30), correspondingly changes its form. In the low pressure limit (large bubbles) when the Van-der-Waals equation transforms into the ideal gas law, the bubble growth equation takes the form

$$dR/dt \approx D_g c_g(1 - R_{cr}/R)kT/2\gamma = D_g(\Delta - \sigma/R)kT/2\gamma, \quad (31)$$

which has a different power dependence on R in the r.h.s., loosing the analogy with the Lifshitz–Slyozov theory. For this reason, one should expect also an other power dependence on time in the final asymptotic formulas of the theory.

For the semi-quantitative analysis of the experiments [33,29] in which the mean bubble radius increased up to $\approx$2–5 nm [33] and 2.5–3.3 nm [29] during the annealing stage, one should take into account that the formal application of the Lifshitz–Slyozov theory results is only partially valid (until $R \ll 5$ nm). For the further analytical consideration this limitation will be ignored, keeping in mind that such a simplified procedure allows only a rough evaluation of the final system state.

The above introduced parameters Δ, σ and R_{cr} completely determine the long-term asymptotic behaviour of the system. The characteristic time scale of the thermal coarsening problem is

$$\tau^* = R_{cr}^3(0)/D_g\sigma,$$

where $R_{cr}(0)$ is the critical radius value in the beginning of this stage, $t = 0$. Since the thermal coarsening commences when $R_{cr} \approx \overline{R}$, the value $R_{cr}(0)$ can be satisfactorily estimated as $\approx$1 nm (see Section 4.2). Using the above estimated value of $(p_s/c_s) \approx 3 \times 10^{13}$ Pa and $D_g \approx$

2×10^{-14} cm^2/s, one obtains $\sigma \approx 0.5\times10^{-11}$ cm and the characteristic time scale $\tau^* \approx 5\times10^3$ s. Since the annealing time (1.8×10^4 s) is somewhat larger than this time scale, the asymptotic expressions of the Lifshitz–Slyozov theory derived in the limit $t \gg \tau^*$ can be used for the approximate description of the final state of the bubble system:

$$\rho_b(t) \approx 0.5Q/2D_g\sigma t, \tag{32}$$

where ρ_b is the intragranular bubble number density, Q is the total concentration of gas atoms in the bulk of the grain in the thermal coarsening stage (including gas atoms both in the grain matrix and in the intragranular bubbles), and

$$\overline{R} \approx (8\sigma D_g t/9)^{1/3}. \tag{33}$$

Since the fission gas release at $T = 900$°C [33] and 700°C [29] in the irradiation stage of the tests was negligibly small (in comparison with the total generated amount of $\approx 5\times10^{19}$ atoms/cm^3) and the grain boundary bubbles had a rather small number density, practically all generated gas was in the bulk of the grains (in the matrix and intragranular bubbles) at $t = 0$, corresponding to $Q \approx 2\times10^{-3}$. Therefore, according to Eqs. (32) and (33) in the end of the annealing stage ($t \approx 1.8\times10^4$ s) the bubble number density and the mean bubble radius attain the values $\rho_b^{(f)} \approx 2.5\times10^{17}$ cm^{-3} and $\overline{R}^{(f)} \approx 1.2$ nm, in noticeable disagreement with the measured values $\rho_b^{(f)} \approx 2.4\times10^{16}$ cm^{-3} and $\overline{R} \approx$ 2–5 nm.

However, an agreement can be much better if one takes into consideration that during the initial stage of annealing, $\tau_s \leqslant 10^3$ s, a significant reduction of the gas atom concentration c_g occurs. Simultaneously such defects as vacancy clusters (up to several nm in diameter, $\leqslant D_u\tau_s$), stacking fault tetrahedra, etc. which were formed under irradiation damage and afforded strong trapping of gas atoms [14], are recovered during this time interval. In this case the diffusion coefficient of gas atoms may significantly increase and approach to its 'unperturbed' value measured in the tests with low damage and gas concentration [14,27]. At 1500°C, the unperturbed diffusion coefficient is about 4×10^{-12} cm^2/s [14], hence, using an intermediate value for D_g in the range between two limiting values, 2×10^{-14} and 4×10^{-12} cm^2/s (say, $D_g \approx 2\times10^{-13}$ cm^2/s), one can get an excellent agreement for the calculated bubble size ($\overline{R}^{(f)} \approx$ 2.6 nm) and number density ($\rho_b^{(f)} \approx 2.5\times10^{16}$ cm^{-3}) with the measurements [29,33]. Further improvement can be attained if bubble collisions will be additionally taken into consideration. In this case thermal coarsening occurs simultaneously with the bubble coagulation process and thus results in increased bubble sizes and decreased bubble number densities.

With the increase of annealing time and temperature, the effect of thermal coarsening becomes more pronounced. Indeed, in this case the mean bubble radius can exceed the above mentioned value 5 nm, and the bubble radius growth will occur much quicker in accordance with Eq. (31). Under the main condition of the Lifshitz– Slyozov theory, $R_{cr} \approx \overline{R}$, it is straightforward to show that Eq. (32) conserves its form:

$$\rho_b(t) \propto Q/\sigma D_g t,$$

whereas Eq. (33) transforms into a new one:

$$\overline{R}^2 \propto t(D_g\sigma kT/\gamma\Omega),$$

corresponding to a more rapid radius growth. In this case after annealing at 1500°C during 72 h the mean bubble diameter can increase up to 100 nm in accordance with observations [38].

Generally, on the base of the above presented qualitative analysis one can conclude that the thermal resolution process becomes essential for the description of the annealing tests, and additionally confirms the necessity of the corresponding thermal term introduction in the code equations (e.g. the third term in the r.h.s. of Eq. (29)).

5. Intergranular porosity

As in the case of the intragranular porosity (see Section 2.1), the evolution of the intergranular porosity is usually considered in the quasi-stationary approximation of mechanical equilibrium bubbles (e.g. [1–3,9,39,40]. Such an approximation is based on the theoretical work [41], in which the kinetics of the intergranular bubble growth determined by the diffusional flux of the grain boundary vacancies was considered. According to [41], the grain boundary vacancy flux is evaluated as

$$\begin{aligned} J_{g.b.} &\approx (2\pi w/L)D_v^{g.b.}(c_v^{eq} - c_v(\rho)) \\ &= (2\pi w/L)D_v^{g.b.}c_v^{eq}\{1 - \exp[(p - p_h - 2\gamma/\rho)\Omega/kT]\} \\ &\approx -(2\pi w/L)D_u^{g.b.}(p - p_h - 2\gamma/\rho)\Omega/kT, \end{aligned} \tag{34}$$

where $D_v^{g.b.}$ is the grain boundary vacancy diffusion coefficient, $D_u^{g.b.} = D_v^{g.b.}c_v^{eq}$ is the grain boundary self-diffusion coefficient, w is the boundary thickness, ρ is the radius of curvature of the pore, $L \approx 1$ is a function of the fraction of the grain boundary area occupied by pores; thus, the quasi-stationary state ($J_{g.b.} = 0$) corresponds to the mechanically stable bubble:

$$p - p_h - 2\gamma/\rho = 0. \tag{35}$$

However, applying these results to the UO_2 fuel it was generally ignored that the original model [41] did not consider an irradiated crystal. Under non-equilibrium conditions of the irradiated crystal the vacancy concentration in the grain bulk may be so high that the

vacancy flux J_g from the interior of the grain to the boundary exceeds the grain boundary vacancy flux $J_{g.b.}$.

In order to determine the applicability range of the standard approach, one should compare the two fluxes. In accordance with Eq. (4):

$$\begin{aligned} J_g &= 4\pi\rho D_v c_v\{1-\beta_i/\beta_v-(c_v^{eq}/c_v) \\ &\quad \exp[(p-p_h-2\gamma/\rho)\Omega/kT]\} \\ &\approx 4\pi\rho D_v c_v^{eq}[(1-\beta_i/\beta_v)(c_v/c_v^{eq}) \\ &\quad -1-(p-p_h-2\gamma/\rho)\Omega/kT]; \end{aligned} \tag{36}$$

thus, the ratio of the two fluxes is

$$\begin{aligned} J_{g.b.}/J_g \approx (D_u^{g.b.}/D_u)(w/\rho)[(p-p_h-2\gamma/\rho)\Omega/kT]/ \\ [1-(1-\beta_i/\beta_v)(c_v/c_v^{eq}) \\ +(p-p_h-2\gamma/\rho)\Omega/kT]. \end{aligned} \tag{37}$$

As demonstrated above, the radiation effects become negligible at $T \geqslant 1500$°C (in comparison with the thermal ones), and $(1-\beta_i/\beta_v)(c_v/c_v^{eq}) \approx 1$. Therefore, since the value $(D_u^{g.b.}/D_u) \approx 10^5$ is extremely large [42], $J_{g.b.}/J_g \gg 1$ and the approach of [41] can be reliably extended also to the case of the irradiated fuel at $T \geqslant 1500$°C.

However, at lower temperatures, $T < 1500$°C the expression $(1-\beta_i/\beta_v)(c_v/c_v^{eq})$ becomes >1, thus, $J_g \neq 0$ when $p-p_h-2\gamma/\rho = 0$, and the above mentioned quasi-stationary condition $J_{g.b.} = 0$ leads to $J_{g.b.}/J_g \to 0$. This means that in reality the bubble state determined by the capillarity relation Eq. (35) is not stationary but corresponds to the bubble growing due to the diffusional flux of the point defects from the bulk of the grain. Therefore, for instance at 1200°C, when $(1-\beta_i/\beta_v)(c_v/c_v^{eq}) \geqslant 10$, for large bubbles with $\rho \geqslant 10^2$ nm the condition $J_{g.b.}/J_g > 1$ is valid only for $p-p_h \geqslant 10\times(2\gamma/\rho)$, whereas for $\rho \geqslant 1$ μm it is only for $p-p_h \geqslant 10^2\times(2\gamma/\rho)$.

It is quite clear that in such a situation both processes of the bulk and grain boundary point defect diffusion should be considered self-consistently in order to describe the evolution of large intergranular bubbles (with $\rho \gg 10$ nm). Such a consideration shows that the bulk diffusion starts to dominate already at 1300–1400°C, This allows the description of the large intergranular bubble evolution by a line of the type represented by the dashed line in Fig. 3. Indeed, since the internal pressure in such bubbles is rather small (in comparison with the capillary one, see Section 2.3.2), then, as seen from Eq. (37), the grain boundary vacancy flux turns to be really negligible in comparison with the bulk one. Hence, for instance at 1300°C, $[(2\gamma/\rho)-p]\Omega/kT \approx (2\gamma/\rho)\Omega/kT \approx 10^{-2}$ for $\rho \approx 1$ μm; therefore, $J_{g.b.}/J_g \approx 10^{-1}$. The maximum size of bubbles growing by the grain boundary diffusional mechanism also quickly decreases with the temperature decrease. Thus, the growth of all the intergranular bubbles with $\rho > 10$ nm can be described at temperatures below 1100°C neglecting the grain boundary vacancy diffusion flux, i.e. the standard approach based on the equilibrium crystal model [41] is not valid in this temperature range.

Since in this case (corresponding to the dashed line in Fig. 3) the kinetics of the bubble size growth are determined by the point defect flux rather than by the gas atom flux (as it was in the standard approach, see Section 2.3.2), the bubble growth rate becomes significantly higher. For the same reason, the internal pressure in such bubbles is rather low (in comparison with the capillary one). Both these factors can lead to a significant underestimation of the value and rate of the fuel swelling by the standard models, and can radically change the behaviour of the system even qualitatively. For instance, during formation of the open porosity on the grain faces, the channels formed by the bubble chains will practically conserve their form after the gas release from these bubbles (see dash–dotted line in Fig. 3) and will not shrink (as in the models for the 'capillary' bubbles, e.g. [9]). This in its turn will additionally increase the gas release rate from the fuel.

6. Conclusions

In the present paper the standard approaches for modelling of the inter- and intragranular bubbles evolution in the UO_2 fuel are critically analysed on the basis of the available experimental data. It is demonstrated that the main source of errors in the simplified treatment of the problem by the standard models can be associated with the underestimation of

- the radiation effects at temperatures below ≈1500°C (where these effects dominate over the thermal ones);
- the thermal effects at temperatures above ≈1500°C (where these effects dominate over the radiation ones).

At low temperatures ($\leqslant 1500$°C) the generally accepted quasi-stationary approximation based on the capillarity relation for growing bubbles fails, since non-equilibrium point defects generated in the fuel under irradiation conditions significantly change the behaviour of growing bubbles at these temperatures, especially in the case of large bubbles formed on the grain faces or during transients in the bulk of the grains. In particular, this may lead to a significant underestimation of the value and rate of the fuel swelling. On the other hand, the presented analysis of the defect structure evolution allows a quantitative description of the bubble nucleation mechanism, as well as the evaluation of the bubble number density and stable size attained under steady irradiation conditions.

At high temperatures ($\geqslant 1500$°C) the thermal resolution of gas atoms from bubbles generally unaccounted in the standard models, becomes the dominant process leading to a significant increase of the critical nucleus of

bubbles and, as a result, change of the mechanism and kinetics of the bubble generation. On the other hand, a self-consistent consideration of the thermal and radiation-induced resolution processes allows a natural explanation and a quantitative description of the bubble size and the number stabilisation observed also at high temperatures under steady irradiation conditions. Under post-irradiation annealing conditions the thermal mechanism determines coarsening (Ostwald ripening) of bubbles and allows a satisfactory description of the high temperature annealing tests.

Acknowledgements

The author thanks Dr Hj. Matzke (TUI, Karlsruhe) for his kind response and comments to the pre-print version [43] of this paper, and V. Kulik for performance of numerical calculations (Figs. 7–10). This work was partially supported by IPSN-CEA, Cadarache (France) under the Contract No. 4000 8A 575 900 on the mechanistic code MFPR development; the personal interest of Dr M. Kissane (IPSN) is acknowledged.

References

[1] J. Rest, GRASS-SST: A comprehensive mechanistic model for the prediction of fission-gas behaviour in UO2- Base fuels during steady-state and transient conditions. NUREG/CR-0202, ANL-78-53, 1978.
[2] J. Rest, S.A. Zawadzki, FASTGRASS: A mechanistic model for the prediction of Xe, I, Cs, Te, Ba, and Sr Release from Nuclear Fuel under Normal and Severe-Accident Conditions, NUREG/CR-5840,ANL-92/3, 1992.
[3] T.J. Heames, D.A. Williams, N.E. Bixler, A.J. Grimley, C.J. Wheatley, N.A. Johns, P. Domogala, L.W Dickson, C.A. Alexande, I. Osborn-Lee, S. Zawadzki, J. Rest, A. Mason, R.Y. Lee, VICTORIA: A mechanistic model of radionuclide behaviour in the reactor coolant system under severe accident conditions, NUREG/CR-5545, 1992.
[4] J.L Katz, H. Wiedersich, J. Chem. Phys. 55 (1971) 1414.
[5] K.C. Russell, Acta Metall. 26 (1978) 1615.
[6] L.K. Mansur, M.H. Yoo, J. Nucl. Mater. 74 (1978) 228.
[7] C.C. Dollins, F.A. Nichols, J. Nucl. Mater. 91 (1976) 143.
[8] M.H. Wood, J.R. Matthews, J. Nucl. Mater. 91 (1980) 35.
[9] R.J. White, M.O. Tucker, J. Nucl. Mater. 118 (1983) 1.
[10] E.E. Gruber, The role of bubble-size equilibration in the transient behaviour of fission gas, ANL-78-36, 1978.
[11] M.W. Finnis, M.R. Hayns, R. Bullough, The Response of Fission Gas Bubbles to Rapid Heating, AERE-R-7970, 1975.
[12] M.E. Gulden, J. Nucl. Mater. 23 (1967) 30.
[13] C. Baker, J. Nucl. Mater. 71 (1977) 117.
[14] Hj. Matzke, in: S.E. Donnelly, J.H. Evans (Eds.), Fundamental aspects of Inert Gases in Solids, Plenum, New York, 1991, p. 401.
[15] I.R. Brearlet, D.A. MacInnes, J. Nucl. Mater. 95 (1980) 239.
[16] C.A. Parker, K.C. Russell, Scripta Met. 15 (1981) 643.
[17] A.D. Whapham, B.E. Sheldon, Electron microscope observation of the fission-gas bubble distribution in UO2, AERE-R-4970, 1965.
[18] R.M. Cornell, J. Nucl. Mater. 38 (1971) 319.
[19] A.J. Manley, Gas bubbles and porosity in irradiated UO2, TRG-2539 (S), 1974.
[20] C. Baker, J. Nucl. Mater. 66 (1977) 283.
[21] Yu.G. Degaltsev, N.N. Ponomaryov-Stepnoy, V.F. Kuznetsov, Behaviour of High Temperature Nuclear Fuel Under Irradiation, Moscow, 1987 (in Russian).
[22] L.D. Landau, E.M. Lifshitz, Hydrodynamics, Moscow, 1986 (in Russian).
[23] A.V. Palagin, private communication.
[24] I.L.F. Ray, H. Thiele, H. Matzke, J. Nucl. Mater. 188 (1992) 90.
[25] A.D. Brailsford, R. Bullough, Philos. Trans. Royal Soc. A 302 (1981) 87.
[26] H. Matzke, Adv. Ceram. 17 (1986) 1.
[27] H. Matzke, Radiat. Eff. 53 (1980) 219.
[28] R. Bullough, M.R. Hayns, J. Nucl. Mater. 55 (1975) 237.
[29] J.A. Turnbull, R.M. Cornell, J. Nucl. Mater. 36 (1970) 161.
[30] J.A. Turnbull, R.M. Cornell, J. Nucl. Mater. 41 (1971) 156.
[31] J.A. Turnbull, J. Nucl. Mater. 38 (1971) 203.
[32] J.A. Turnbull, Radiat. Eff. 53 (1980) 243.
[33] S.R. Pati, M.J. Dapht, D.R. OBoyle, J. Nucl. Mater. 50 (1974) 227.
[34] M. Hirai, J.H. Davies, R. Williamson, J. Nucl. Mater. 226 (1995) 238.
[35] V.V. Surenyanz, Z. Fiz. Khim. 45 (1971) 2985 (in Russian).
[36] R.M. Cornell, J.A. Turnbull, J. Nucl. Mater. 41 (1971) 87.
[37] E.M. Lifshitz, L.P. Pitaevsky, Physical Kinetics, Moscow, 1979 (in Russian).
[38] A.M. Ross, J. Nucl. Mater. 30 (1969) 134.
[39] M.O. Tucker, J. Nucl. Mater. 78 (1978) 17.
[40] J.R. Matthews, M.H. Wood, J. Nucl. Mater. 91 (1980) 241.
[41] M.V. Speight, W. Beere, Met. Sci. 9 (1975) 190.
[42] C.B. Alcock, R.J. Hawkins, A.W.D. Hills, P. McNamara, Paper SM-66/36, IAEA, Symp. Thermodynamics. Vienna, 1965, p. 57.
[43] M.S. Veshchunov, Development of the theory of fission gas bubble evolution in irradiated UO2 Fuel, Preprint IBRAE-98-11, Moscow, 1998.